Sensors and Actuators B 233 (2016) 180–192

Contents lists available at ScienceDirect

Sensors and Actuators B: Chemical

journal homepage: www.elsevier.com/locate/snb

Synthesis and improved gas sensing properties of NiO-decorated SnO_2 microflowers assembled with porous nanorods

Guang Sun[a,*], Honglin Chen[a], Yanwei Li[a], Zehua Chen[a,*], Saisai Zhang[a], Guangzhou Ma[a], Tiekun Jia[b], Jianliang Cao[a], Hari Bala[a], Xiaodong Wang[a], Zhanying Zhang[a]

[a] School of Materials Science and Engineering, Cultivating Base for Key Laboratory of Environment-friendly Inorganic Materials in University of Henan Province, Henan Polytechnic University, Jiaozuo 454000, PR China
[b] Department of Materials Science and Engineering, Luoyang Institute of Science and Technology, Luoyang 471023, PR China

ARTICLE INFO

Article history:
Received 3 November 2015
Received in revised form 29 March 2016
Accepted 9 April 2016
Available online 12 April 2016

Keywords:
Porous structure
NiO/SnO_2
Sacrificial template
Heterojunction
Gas sensor

ABSTRACT

Aiming to improve the gas sensing property of SnO_2 by utilizing the advantages of both porous structure and p-n junctions, NiO-decorated SnO_2 microflowers assembled with porous nanorods were successfully prepared via a sacrificial template-assisted synthesis method by using SnC_2O_4 as sacrificial template for porous SnO_2 and $Ni(NO_3)_2$ as NiO source. Through this method, different amounts of NiO can be homogenously dispersed in porous SnO_2 to form p-NiO/n-SnO_2 junctions without changing the original flower-like morphology of SnC_2O_4. In the as-prepared flower-like NiO/SnO_2 architecture, the porous nanorods are about 2 μm in length and 100–200 nm in diameter and are constructed by numerous loosely stacked nanoparticles with the size about 20 nm. Gas sensing tests indicate that the NiO/SnO_2 microflowers exhibit a remarkably improved gas sensing performance compared with pristine SnO_2. The response of 1NTO (with the optimal NiO content of 1 mol%) to 1000 ppm ethanol is as high as 576.5, which is much higher than that of the pristine SnO_2 (315.5). Besides of high sensitivity, the 1NTO sensor also exhibits excellent linearity in a wide range of ethanol concentration (50–1000 ppm) as well as good repeatability and durability. The p-NiO/n-SnO_2 heterojunction related gas sensing mechanism was discussed.

1. Introduction

Detecting the existence and concentration of flammable, explosive or toxic gases plays a crucial role in human safety and environment protection. In the past decades, metal oxide semiconductor (MOS) based gas sensor has attracted much attention owing to the merits of low cost, easy fabrication, and good response to a wide range of gases. Developing novel MOS sensing materials with high performance to make MOS sensor more suitable for practical application has long been a hot topic in the field of gas sensor field [1–5].

Tin oxide (SnO_2), as a well-known *n*-type MOS with a wide band gap of 3.6 eV, has been intensively studied due to its diverse functions and potential applications in photocatalyst [6], lithium ion battery [7–9] and solar cells [10,11]. Particularly, SnO_2 has good capacity to response to many reducing and oxidizing gases and thus is regarded as one of the most promising gas sensing materials [12–16]. Recently, aiming to improve the gas sensing performance, many researchers have devoted their efforts on fabricating SnO_2 micro/nanostructure with novel morphology because of its prominent morphology-dependent property [17–22]. Among various micro/nanostructure, porous SnO_2 micro/nanostructures have been considered as a promising family for achieving high sensing performance [13,23–28]. A great number of pores contained in porous micro/nanostructures can provide enough channels for gas diffusion and transport. Moreover, their rough surface and large specific surface area can provide more active sites for gas adsorption and subsequent surface reaction. Such characteristics can always endow SnO_2 with enhanced gas sensing properties. For example, Huang et al. reported the synthesis of porous SnO_2 microcubes with enhanced ethanol and formaldehyde sensing property via hydrothermal acid-washing Mn_2O_3/SnO_2 hybrids [23]; Jin et al. prepared the nanoparticle-assembled porous SnO_2 microspheres with enhanced ethanol sensitivity by using biopolymer sodium alginate as the structure-directing agent [24]; Xu et al. reported the fabrication of hierarchical porous SnO_2 microrods through topological transformation of tin oxalate and applied them in gas sensor for fast detecting trace formaldehyde [27]. Besides of fabricating novel micro/nanostructures, the construction of oxide

* Corresponding authors.
E-mail addresses: mcsunguang@163.com (G. Sun), zehua_c@yahoo.com (Z. Chen).

http://dx.doi.org/10.1016/j.snb.2016.04.057
0925-4005/

heterojunctions in SnO_2 by introducing a proper amount of foreign p- or n-type MOS can also improve the sensor response [29–35]. Choi et al. reported that the response of SnO_2 nanowire to reducing gases like H_2 and CO can be remarkably enhanced by surface functionalization with Cr_2O_3 nanoparticles (NPs) [29]; Ju et al. reported that the NiO/SnO_2 hollow spheres consisting of p-NiO/n-SnO_2 junctions exhibited much higher response to triethylamine than the pristine SnO_2 hollow spheres [30]; In our previous work, we found that through decorating SnO_2 nanosheets with discrete ZnO NPs, the response of the SnO_2 microflower built of nansosheets was improved due to the formation of ZnO-SnO_2 heterojunctions [32]. All these results clearly demonstrated that fabricating porous structure and constructing oxide heterojunctions are of two effective strategies to improve the gas sensing performance of SnO_2. As an extension of above two strategies, it is reasonable to believe that superior gas sensing performance can be achieved by integrating the advantages of porous structure and heterojunctions in SnO_2. However, to the best of our knowledge, in contrast with the abundant reports on porous SnO_2, the researches on the synthesis and gas sensing property of the porous NiO/SnO_2 nanocomposites are relatively rare, especially the heterostructured NiO/SnO_2 microflowers assembled with porous nanorods.

Following above-mentioned thought, in this paper, NiO-decorated SnO_2 microflowers built of porous nanorods were fabricated via a reliable two-step route by using self-synthesized SnC_2O_4 as sacrificial template, and characterized by X-ray diffraction (XRD), filed-emission electron scanning microscopy (FESEM), energy dispersive spectroscopy (EDS) and transmission electron microscopy (TEM). The gas sensing properties of the prepared samples were investigated in detail. It was found that the as-prepared heterostructured NiO/SnO_2 microflowers showed superior ethanol sensing performances to the pristine SnO_2 counterpart. The possible improved gas sensing mechanism was discussed in relation with p-NiO/n-SnO_2 heterojunctions.

2. Experimental

2.1. Materials

All of the chemical reagents in experiments, including stannous chloride dihydrate ($SnCl_2{\cdot}2H_2O$), oxalate dehydrate ($H_2C_2O_4{\cdot}2H_2O$), polyethylene glycol (PEG-400) and absolute ethanol, are of analytical grade and used as received without any further purification.

2.2. Preparation of SnC_2O_4 sacrificial template

Flower-like SnC_2O_4 microstructure was synthesized through a PEG-assisted precipitation method. In a typical procedure, 6.1 g $H_2C_2O_4{\cdot}2H_2O$ was first dissolved in a mixed solvent of ethanol (130 mL) and PEG-400 (40 mL). Then, 7.2 g $SnCl_2{\cdot}2H_2O$ was introduced into the solution under magnetic stirring, followed by adding 20 mL deionized water drop by drop. After continuously stirring for 90 min, the produced white precipitate was collected by centrifugation, washed with distilled water and ethanol for several times, and finally dried in air at 60 °C for 5 h.

2.3. Preparation of NiO-decorated SnO_2 microflowers

In a typical synthesis procedure, 2 g as-syntheiszed SnC_2O_4 powder was added into 10 mL aqueous solution containing a designed amount of $Ni(NO_3)_2$ under magnetic stirring. After stirring for 5 min, the above mixture solution was ultrasonically treated for another 10 min, and then heated at 70 °C to remove the solvent. Finally, the obtained mixed powder was calcined in air at 500 °C for 2 h to obtain the NiO/SnO_2 composite. The NiO content can be precisely controlled by tuning the amount of $Ni(NO_3)_2$. The composites with the NiO contents of 0.75 mol%, 1 mol% and 1.25 mol% were successfully prepared and denoted as 0.75NTO, 1NTO and 1.25NTO, respectively. In addition, pure SnO_2 was also prepared by directly annealing SnC_2O_4 in absence of $Ni(NO_3)_2$. The whole synthesis process is schematically illustrated in Fig. 1.

2.4. Characterization

The phase structure and purity of the prepared samples were investigated by powder X-ray diffraction (XRD) using a Bruker/D8-Advance diffractometer with Cu Kα radiation. The morphology and microstructure were investigated by field emission scanning electron microscopy (FESEM, Quanta 250 FEG) and transmission electron microscopy (TEM, JEOL, JEM-2100). Elemental analysis was performed by energy dispersive spectroscopy (EDS, INCA ENERGY 250) integrated into the FESEM system. The differential thermal analysis (DTA) and thermogravimetric analysis (TGA) were carried out on a Setaram Evolution 2400 thermal analyzer. The specific surface area of the prepared samples was measured on a Micromeritics Triatar 3020 apparatuses by using Brunauer-Emmett-Teller (BET) method. UV–vis adsorption spectra were obtained on a UV–vis diffuse reflection spectrometer (TU1901).

2.5. Sensor fabrication and measurement

A proper amount of as-prepared sample was mixed with several drops of distilled water in an agate mortar to form a homogeneous past, which was then coated onto a ceramic substrate (13.4 mm × 7 mm, screen-printed with Ag-Pd comb-like electrodes) to obtain the resistance-type sensor. The gas-sensing properties of the sensor were tested on an intelligent gas sensing analysis system of CGS-4TPS (Beijing Elite Tech. Co., Ltd., China). Before testing, the sensor was aged at 200 °C for 12 h to improve the repeatability and stability. The sensor response (S) was defined as the ratio of R_a/R_g, where R_a and R_g were the electrical resistance of sensor in air and in target gas, respectively. The response and recovery times were defined as the time required for a change in response to reach 90% of the equilibrium value after injecting and removing the detected gas, respectively. During the test, the operating temperature range was set at 200–380 °C and the relative humidity was 40%.

3. Results and discussion

3.1. Characterization of the SnC_2O_4 sacrificial template

Fig. 2a shows the XRD pattern of the prepared SnC_2O_4 sacrificial template. All of the diffraction peaks are good agreement with the standard dates of the monoclinic SnC_2O_4 (JPCDS file: No. 510614), and no peaks from other impurities are detected, indicating the formation of crystalline SnC_2O_4 phase with high purity. The FESEM images displayed in Fig. 2b and c reveal that the SnC_2O_4 sample is composed of many ~5 μm flower-like microstructures, which are built of numerous 1D nanorods with the size about 2 μm in length and 100–200 nm in diameter. The TEM image showed in Fig. 2d further indicates that the rod-like petals in the flower-like architecture are of dense and gather together via their bundled ends. The thermal stability of the prepared SnC_2O_4 was investigated, and the obtained DTA-TGA curves are showed in Fig. 3. A strong exothermic peak centered at 292 °C (DTA curve) can be observed. This exothermic process corresponds to a weight loss about 27.4% (TGA curve), being agreement with the theoretical weigh loss (26%) of the decomposition of SnC_2O_4 to produce SnO_2. In our experiment, in order to get better crystalline SnO_2 and simultaneously pre-

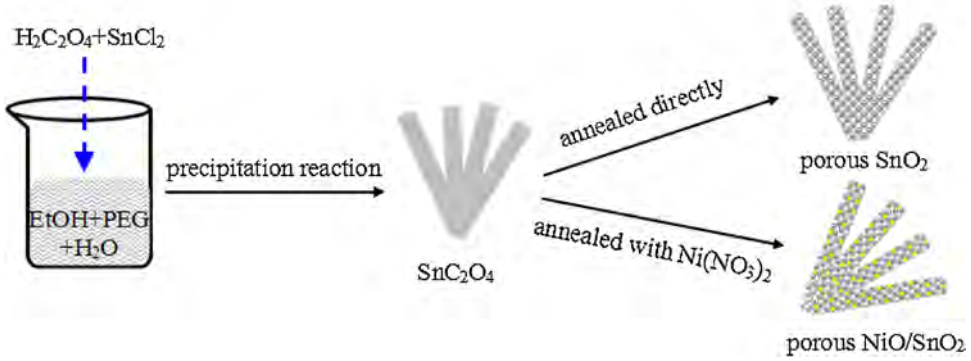

Fig. 1. Schematic illustration for the preparation of flower-like NiO/SnO_2 and SnO_2 architectures assembled with porous nanorods.

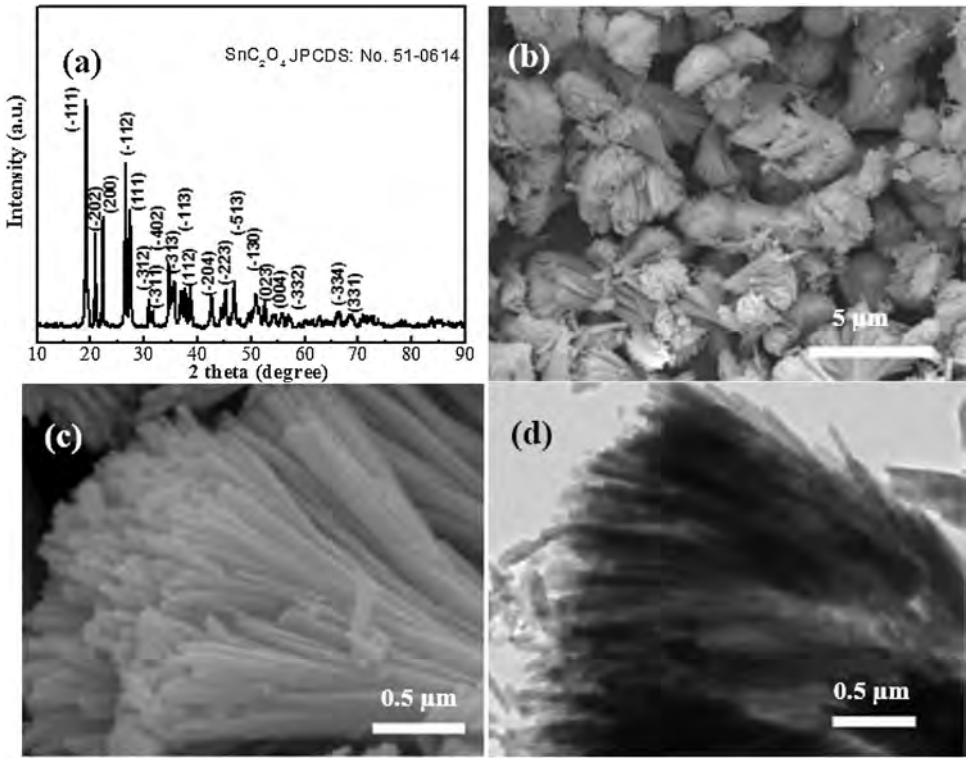

Fig. 2. (a) XRD pattern, (b, c) FESEM and (d) TEM images of the synthesized SnC_2O_4 sacrificial template.

vent the porous structure from collapsing, the following calcination temperature is chosen at 500 °C.

3.2. Characterization of the flower-like microstructure of SnO_2 and NiO/SnO_2

Considering that SnC_2O_4 can decompose to SnO_2 at the temperature above 292 °C, the present flower-like SnC_2O_4 microstructure provides us an ideal sacrificial template to prepare SnO_2 and NiO/SnO_2. Thus, by annealing SnC_2O_4 with or without $Ni(NO_3)_2$, NiO/SnO_2 composites and pure SnO_2 were prepared, respectively. Fig. 4 displays the XRD patterns of the obtained samples. The diffraction peaks arising from tetragonal rutile SnO_2 (JCPDS file: No. 41-1445) as well as a small diffraction peak arising from orthorhombic SnO_2 (JCPDS file: No. 29-1484) are observed, indicating the formation of crystalline SnO_2 phases in the four samples. However, no obvious peaks related to NiO can be found in 0.75NTO, 1NTO and 1.25NTO, which is probably due to the low content and small crystal size of the NiO dopant. Based on the Scherer formula ($D = \frac{0.9\lambda}{\beta \times \cos\theta}$, where λ is the wavelength of the X-ray beam, β is the full width at half maximum, and θ is the diffraction angle), the average grain sizes of SnO_2 crystallites calculated from (110) plane are 22.7, 19.8, 19.0, 17.7 nm for pure SnO_2, 0.75NTO, 1NTO and 1.25NTO, respectively. With the increase of NiO content, the grain size of SnO_2 was slightly decreased, indicating that the presence of NiO can restrain the growth of SnO_2 crystals.

The FESEM images of the prepared SnO_2 and NiO/SnO_2 composites are presented in Fig. 5a–h. From Fig. 5a, one can clearly see that the flower-like hierarchical microstructures, similar to SnC_2O_4 precursor, were obtained in the pure SnO_2 product, revealing that after a phase transformation from SnC_2O_4 to SnO_2, the SnC_2O_4 precursor can pass its morphology on to SnO_2. While, in sharp contrast with the dense structure of the SnC_2O_4 nanorods (Fig. 2c and d), a plenty of pores are created on the SnO_2 nanorods (Fig. 5b) due to the decomposition of SnC_2O_4. When a small amount of $Ni(NO_3)_2$ was introduced and then annealed together with the SnC_2O_4 precursor, such flower-like hierarchical microstructure that consisting porous nanorods as building blocks can be also obtained in the

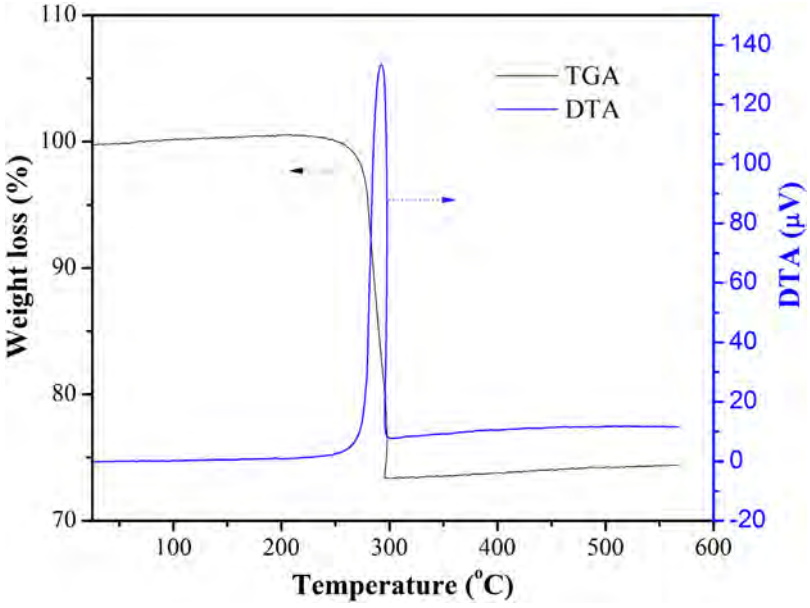

Fig. 3. TGA/DTA curves of the synthesized SnC_2O_4 sacrificial template.

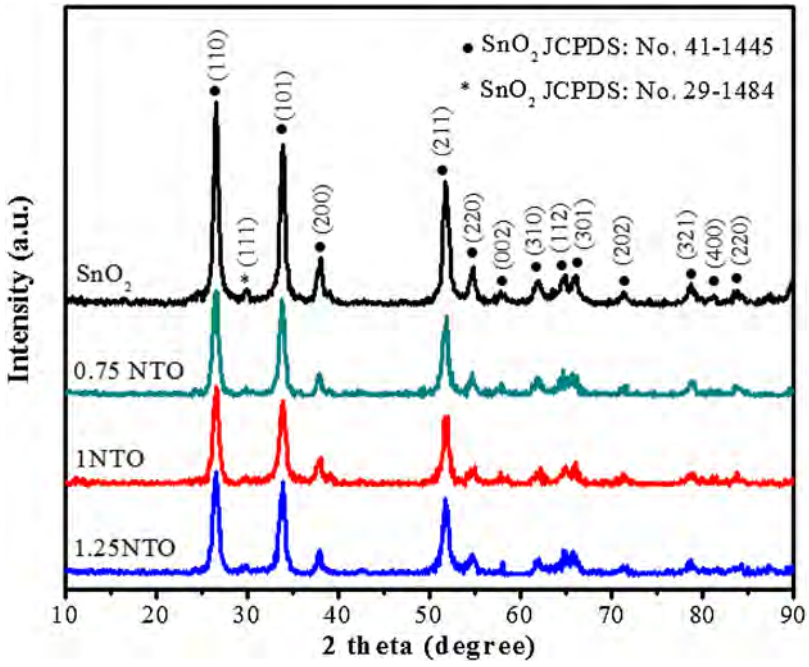

Fig. 4. (a) XRD patterns of the synthesized pure SnO_2, 0.75NTO, 1NTO and 1.25NTO.

final NiO/SnO_2 composites (Fig. 5c–h). Such result indicates that under the present experimental condition the addition of a small amount of $Ni(NO_3)_2$ has almost no impact on the formed morphology of the product. EDS measurements were subsequently carried out to investigate the chemical composition of the porous nanorods. Fig. 5i–k displays the EDS element mappings recorded from Fig. 5f. Three elements of Sn, Ni and O are observed, suggesting that these porous nanorods are composed of SnO_2 and NiO. Moreover, the good dispersion of Ni elements among Sn and O elements indicates that NiO is homogeneously distributed on the porous SnO_2 nanorods.

The obtained NiO/SnO_2 composites were further investigated by TEM. Fig. 6a shows a typical TEM image of 1NTO. Being consistent with above FESEM observation, the flower-like microstructure built of porous nanorods can be clearly observed. From the enlarged TEM image showed in Fig. 6b, it can be further seen that these porous nanorods are constructed by numerous loosely stacked nanoparticles. The average size of these nanoparticels is measured to be about 20 nm, being consistent with the result of XRD analysis. The selected area electron diffraction (SAED) pattern showed in Fig. 6c reveals that these porous nanorods are of polycrystalline in nature. After careful identification, all the diffraction rings from inside to outside can be indexed as the (110), (101), (211), (210) and (002) planes of tetragonal rutile SnO_2 (JCPDS file: No. 41-1445) and (111) and (220) planes of cubic NiO (JCPDS file: No. 78-0643), respectively. The coexistence of crystalline NiO and SnO_2 can be further confirmed by the high resolution TEM (HRTEM) image showed in Fig. 6d. The interplanar distances of 0.33 nm and 0.24 nm are

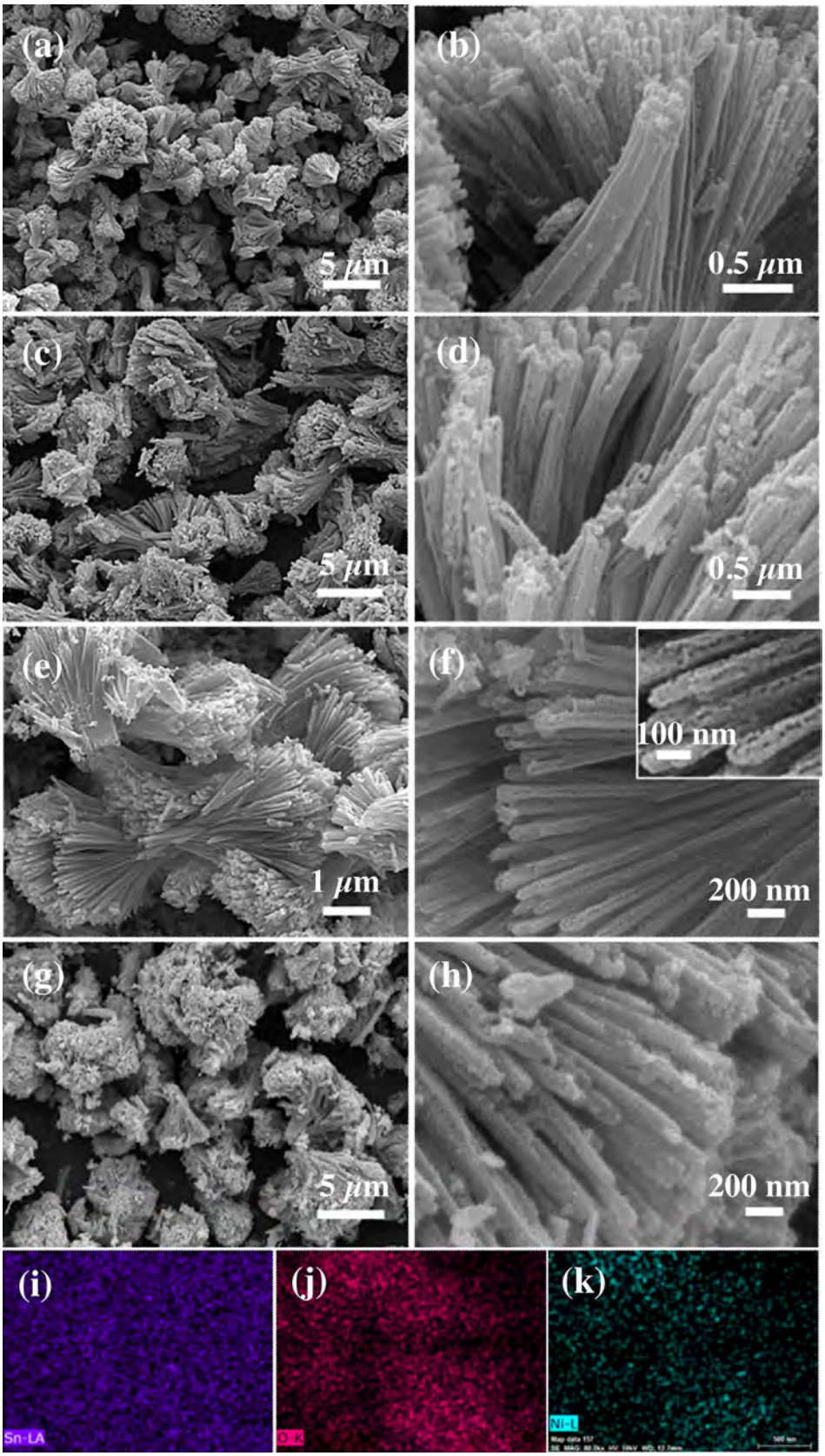

Fig. 5. (a) FESEM images of the synthesized (a, b) SnO_2, (c, d) 0.75NTO, (e, f) 1NTO and (g, h) 1.25NTO and (i–k) the area scanning element mappings of 1NTO recorded from figure (f). The inset of figure (f) is the enlarged FESEM image of 1NTO, clearly demonstrating the formation of porous nanorods.

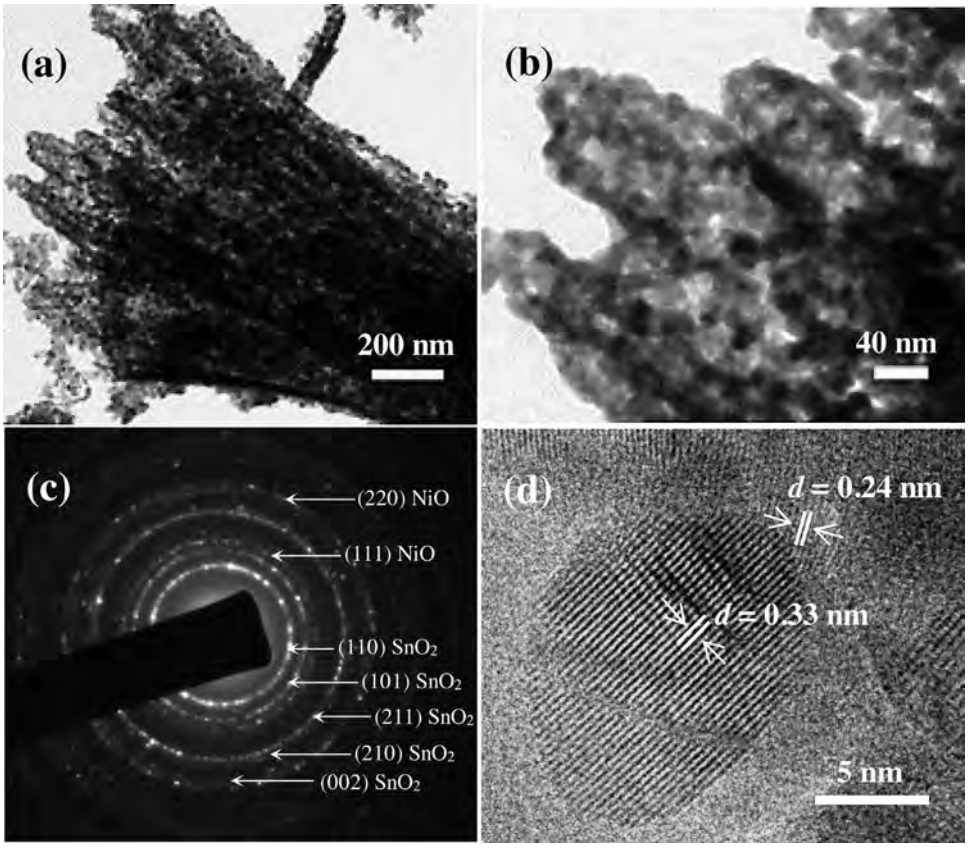

Fig. 6. (a, b) TEM images, (c) SAED pattern and (d) HRTEM image of 1NTO.

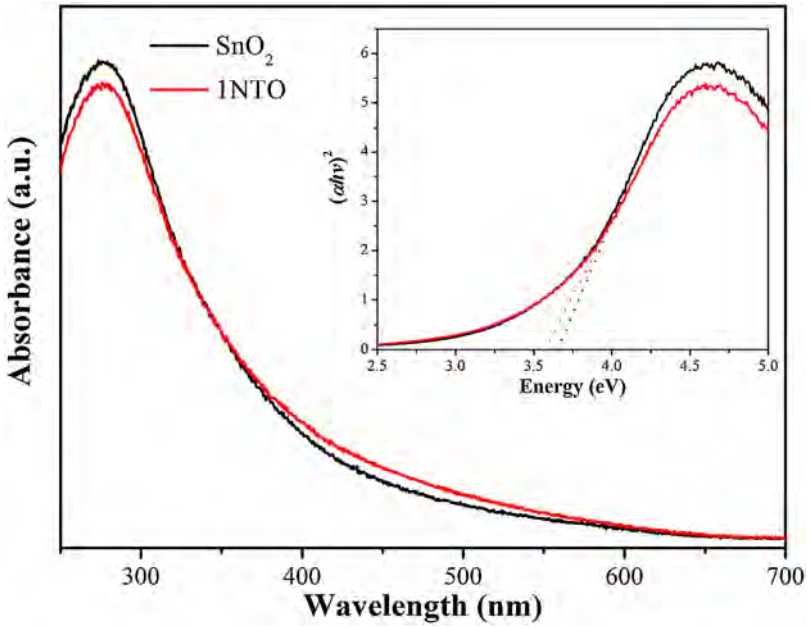

Fig. 7. UV–vis adsorption spectra of the prepared SnO_2 and 1NTO. The inset is the derived plots of $(\alpha h\nu)^2$ versus photon energy ($h\nu$).

close to the *d* values of (110) and (111) planes for tetragonal SnO_2 and cubic NiO, respectively. Moreover, the contacted lattice fringes between NiO and SnO_2 reveal that NiO-SnO_2 heterojunctions were formed in this sample. In principle, the formation of p-n heterojunction (type II) will lead to a narrowed band gap [36]. Thus, in order to further confirm the formation of *p-n* heterojunction in 1NTO, the band gap energies of the prepared SnO_2 and 1NTO were investigated by UV–vis absorption spectra. As shown in Fig. 7, the absorption edge of 1NTO is obviously red shift as compared with that of pure SnO_2. The plots of $(\alpha h\nu)^2$ versus photon energy ($h\nu$) (inset of Fig. 7) were obtained according to the equation of $\alpha h\nu = A\left(h\nu - E_g\right)^{1/2}$, where α, *h*, *ν*, E_g, and A are the absorption coefficient, Planck's constant, light frequency, band gap energy, and a constant, respectively. The band gap energies (E_g) of the prepared

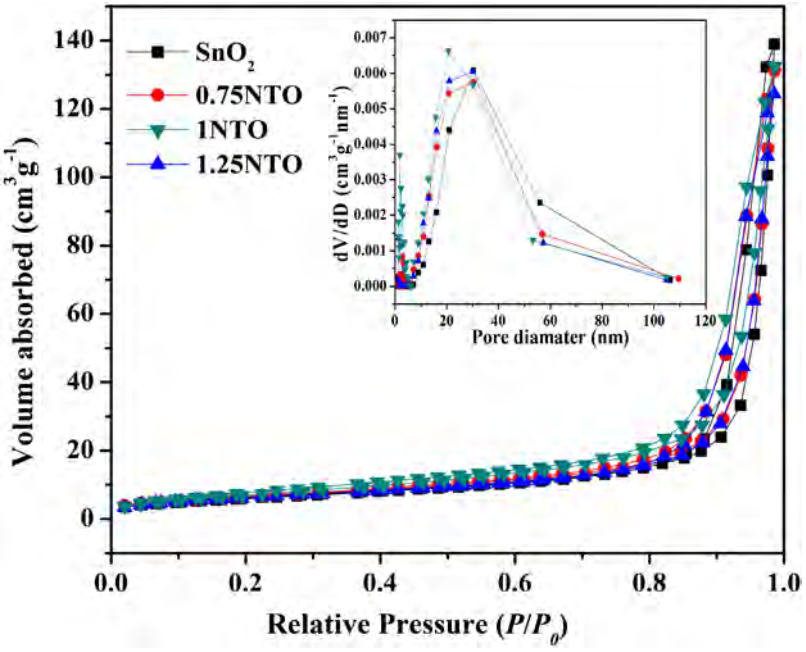

Fig. 8. Nitrogen adsorption-desorption isotherms and corresponding pore size distribution curves (inset) of different samples.

SnO_2 and 1NTO were estimated to be 3.65 and 3.55 eV, respectively. The narrowed band gap of 1NTO further reveals the formation of p-n heterojunction of NiO-SnO_2.

Nitrogen adsorption-desorption measurements were performed on the prepared samples and the results are shown in Fig. 8. All samples exhibit a type of IV isotherm with type H3 hysteresis loop according to IUPAC classification. The BET surface areas are found to be 28.88, 31.16, 32.23 and 32.72 m^2/g for pure SnO_2, 0.75NTO, 1NTO and 1.25NTO, respectively. With the increase of NiO content, the surface area of the samples is only slightly enlarged. The corresponding pore size distribution (inset of Fig. 8) that calculated from the Barret–Joyner–Halenda (BJH) method indicates that the dominant pore size of the four samples are in the range of 10–50 nm. Thus, based on above analysis, we can undoubtedly concluded that heterostructured NiO/SnO_2 microflowers consisting of porous nanorods as building blocks were successfully prepared via the present method.

3.3. Gas sensing properties

The as-prepared NiO/SnO_2 microflowers, possessing the advantages of both porous structure and p-n junctions, were expected to exhibit superior gas sensing properties. So, gas sensing tests were performed on the NiO/SnO_2 composites as well as on the pure SnO_2 for comparison. During the tests, ethanol vapor was chosen as the representative reducing gas. It is well known that the chemical reaction happened on the surface of sensing material is significantly influenced by the operating temperature. Therefore, the temperature-dependent responses of the sensors were first investigated to find the optimum operating temperature. Fig. 9a displays the responses of the sensors toward 300 ppm ethanol vapor at the operating temperature ranging from 200 to 380 °C. The responses of different sensors exhibit similar variations with the increase of temperature, and reach their maximum values at 320 °C. Thus, 320 °C is determined as the optimum operating temperature. At the optimum operating temperature, the responses of pristine SnO_2, 0.75NTO, 1NTO and 1.25NTO are 164.5, 208.1, 257.3 and 185.1, respectively. In general, the response of MOS sensor is closely related with the sensor resistance in air (R_a), which can be severely influenced by many factors, especially including the operating temperature and the heterojunctions. Here, in order to investigate the influence of such two factors on the R_a, the R_a values of pure SnO_2 and 1NTO at different temperature were measured, and the results are showed in Fig. 9b. From this figure, one can see that the R_a values of the two sensors decrease gradually with the increase of temperature, revealing the negative temperature coefficient property of SnO_2 and 1NTO. Moreover, in the whole temperature range, the R_a value of 1NTO is always higher than that of SnO_2. Such result indicates that the R_a value of the present SnO_2 sensor has been increased through the introduction of NiO, which can be attributed to the formation of p-NiO/n-SnO_2 junctions.

Fig. 10 shows the response of the sensors toward varied ethanol concentration at the optimum operating temperature of 320 °C. From Fig. 10a, one can easily see that the responses of all sensors increase very fast with the increase of ethanol concentration before 1000 ppm, but slow down gradually when the ethanol concentration is over 1000 ppm. In the whole concentration range, the NiO/SnO_2 sensors exhibit higher response than the SnO_2 sensor, revealing their superior ethanol sensitivity. In addition, among the three NiO/SnO_2 sensors, the 1NTO sensor shows the best sensitivity to ethanol. For example, the responses of 1NTO to 50 and 5000 ppm ethanol are 94.8 and 1328.4, respectively, which are much higher than that of 0.75NTO (83.1 and 955.1) and 1.25NTO (74.5 and 831.2). Therefore, the optimal NiO content in the present NiO/SnO_2 composite is determined to be 1 mol%. More details about the gas concentration-dependent response variation in the range of 50–1000 ppm are displayed in Fig. 10b. The sensors based on SnO_2, 0.75NTO and 1.25NTO show good linearity from 50 to 500 ppm. In contrast, the linearity range of 1NTO sensor can extent to 1000 ppm. The ethanol sensitivity of 1NTO is compared with that of the NiO/SnO_2 composites reported in literatures. As is shown Table 1, an obvious improvement of ethanol sensitivity was observed for the present 1NTO sensor. The high response and extended linear detection range of 1NTO imply its better capacity in detecting ethanol.

Fig. 11a shows the representative dynamic response-recovery curve of 1NTO sensor to different ethanol concentration at 320 °C. For comparison, the corresponding curve of pure SnO_2 sensor was

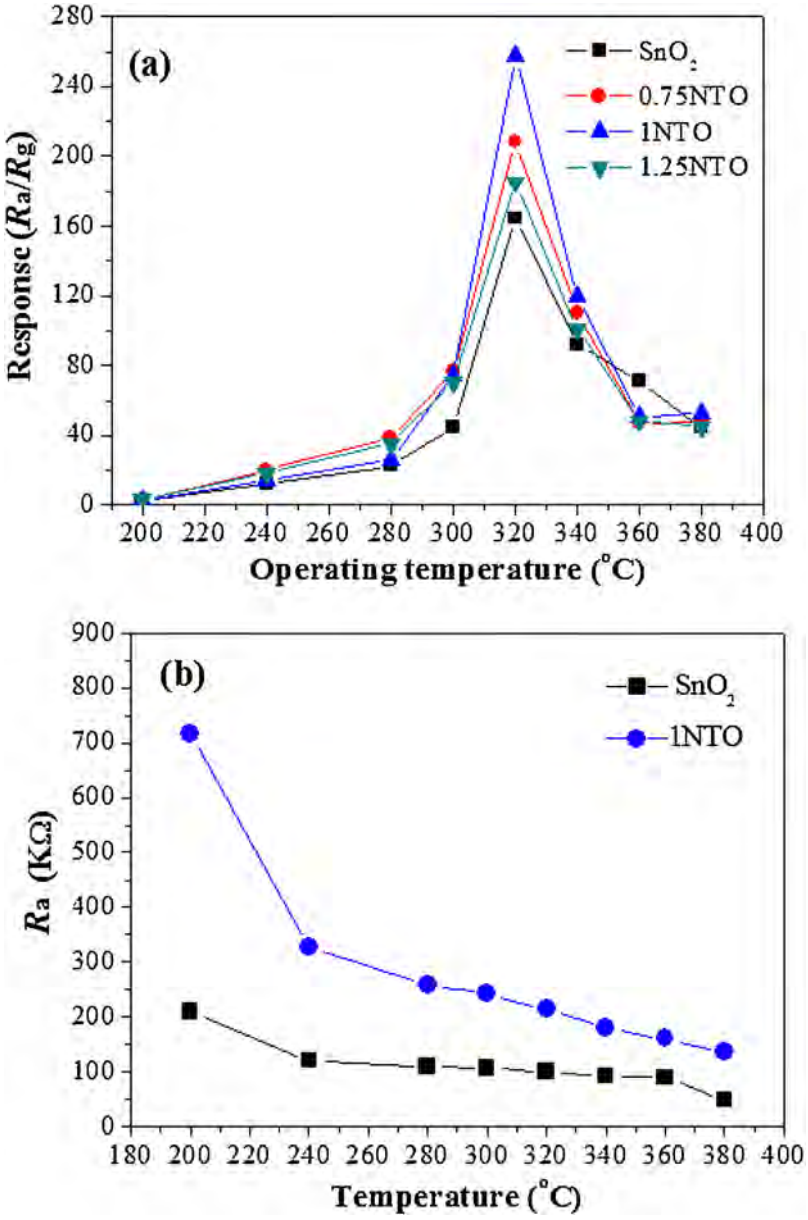

Fig. 9. (a) Response values of the sensors based on SnO_2, 0.75NTO, 1NTO and 1.25NTO to 300 ppm ethanol at different temperatures; (b) the R_a values of pure SnO_2 and 1NTO sensors at different temperatures.

Table 1
Comparison of ethanol sensitivity of NiO/SnO_2 sensors in present work and literatures.

Sensing materials	T (°C)	Ethanol concentration (ppm)	Response (R_a/R_g)	Ref.
NiO/SnO_2 nanofiber	330	50	3.7	[38]
Ni-doped SnO_2 hollow spheres	300	50	14	[39]
NiO-doped SnO_2 nanofibers	200	50	4	[40]
$NiO–SnO_2$ hollow spheres	300	50	12	[41]
NiO/SnO_2 hollow sphere	220	10	4	[30]
1NTO	320	50	94.8	this work

also displayed. Evidently, with the increasing of ethanol concentration, the response amplitude of 1NTO increases gradually. At each tested points the response amplitude of 1NTO is obviously higher than that of SnO_2. Fig. 11b gives the response transient curve of 1NTO sensor to 2000 ppm ethanol at 320 °C. From this figure, the response and recovery times were determined as 9 s and 34 s, respectively. The relatively rapid response and recovery property should be attributed to the unique porous structure of 1NTO. The repeatability and long-term stability of 1NTO were also measured. As shown in Fig. 11c and d, the 1NTO sensor can maintain its initial response without major changes after 4 cycles of measurements and can still keep 85% of initial response value after 30 days, revealing its good repeatability and long-term stability.

The sensitivity of 1NTO sensor were further evaluated by testing its responses toward 300 ppm different reducing gases at 320 °C, and the results are showed in Fig. 12. The responses of 1NTO to all

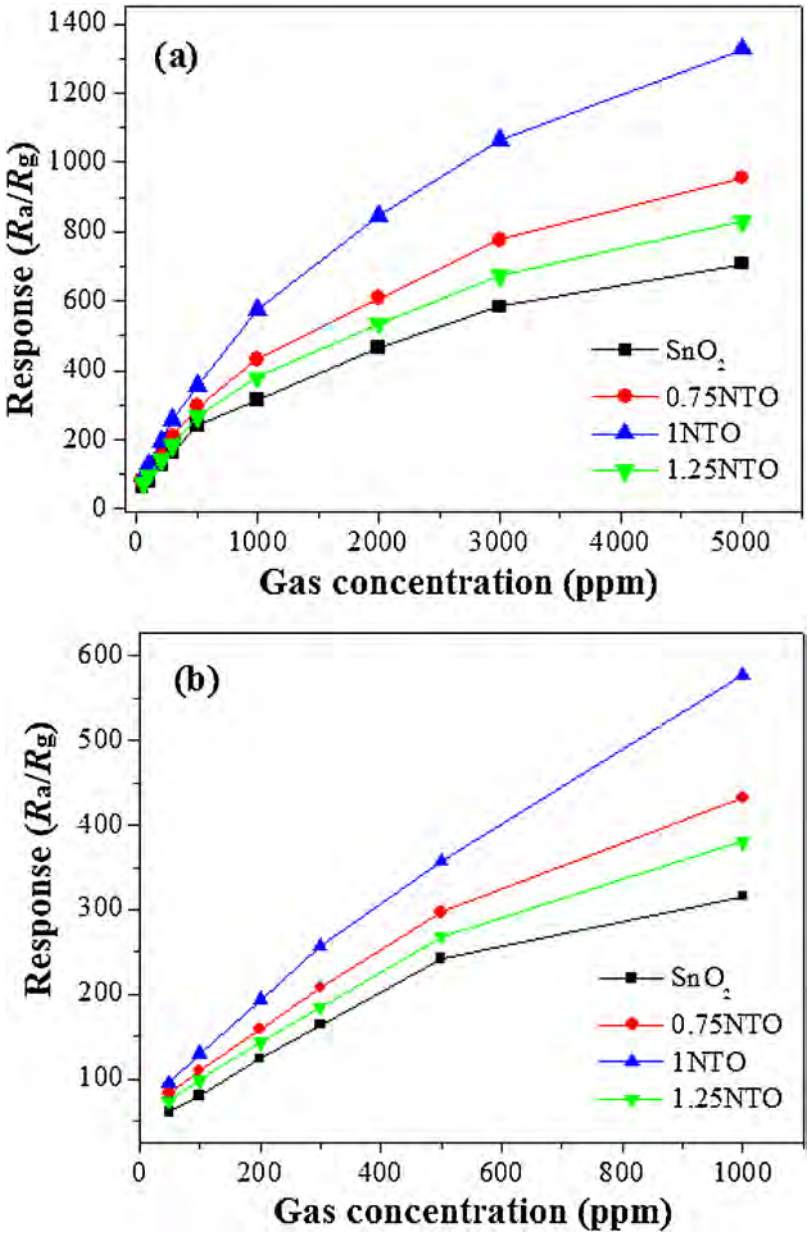

Fig. 10. Response of different sensors versus ethanol concentrations at 320 °C: (a) 50–5000 ppm, (b) 50–1000 ppm.

the tested gases are higher than that of the pure SnO_2 counterpart, suggesting its improved sensitivity to reducing gases. Moreover, the response of 1NTO to ethanol is as high as 257, which is about 3, 4.8, 5.4 and 40.8 times higher than to methanol, acetone, formaldehyde and benzene, respectively, indicating its selectivity to ethanol. The ethanol selectivity of 1NTO sensor may be attributed to the high activity of ethanol molecule that makes it easier to react with absorbed oxygen ions on the surface of sensing materials.

3.4. Mechanism of improved sensing properties

Based on the widely accepted space-charge layer mechanism, the gas sensitivity of MOS is closely related with the electron-depletion layer (EDL) and hole-accumulation layer (HAL) formed on the surface of n- and p-MOS, respectively [2]. As illustrated in Fig. 13a, when the n-SnO_2 sensor is exposed to air, the surface-absorbed oxygen will capture electrons from the conduction band of SnO_2 to generate oxygen anions (O^- is believed to be dominant at the present operating temperature of 320 °C [37]), leading to the formation of EDL on the surface of SnO_2 nanoparticles (NPs). Thus, the conduction channels in SnO_2 NPs are narrowed and the sensor resistance is increased correspondingly. Upon exposure to reducing gas, such as ethanol vapor, the trapped electrons will be released back to SnO_2 due to the redox reaction between ethanol molecules and oxygen anions. As a result, a narrowed EDL and a widened conduction channel are formed, and the sensor resistance is reduced accordingly.

In our experiments, when NiO was dispersed in the SnO_2 porous nanorods, the sensor response is remarkably enhanced. Considering that the pure SnO_2 and NiO/SnO_2 composites have similar porous structure and specific surface areas, the enhanced response should be mainly attributed to the p-n junctions formed between NiO and SnO_2 NPs. Many previous studies have demonstrated that the creation of p-n junctions can enhance the sensor response through changing the width of space-charge layer [29–31]. As shown in Fig. 6d, by decorating porous SnO_2 nanorods with NiO NPs,

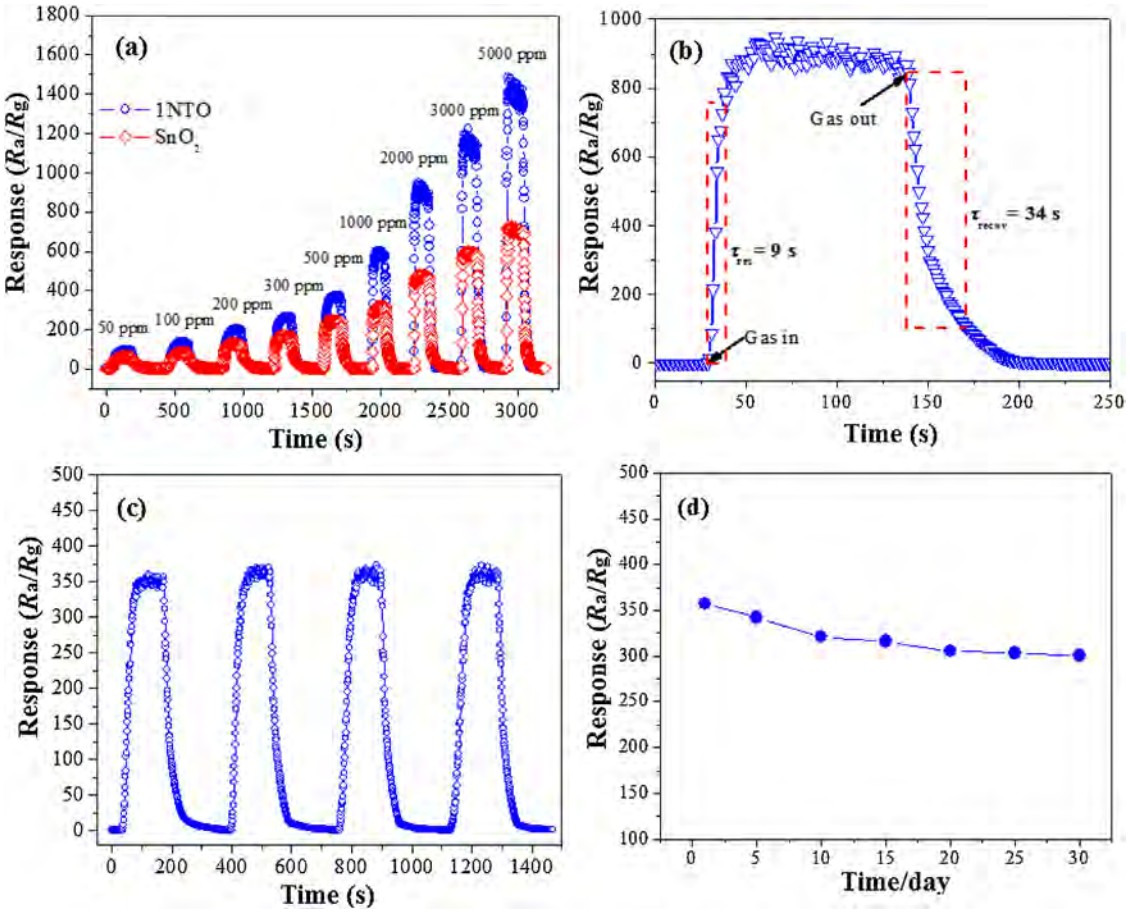

Fig. 11. (a) Real time response curves of the pure SnO_2 and 1NTO to ethanol in the range of 50–5000 ppm; (b) response-recovery curve of 1NTO to 2000 ppm ethanol; (c) repeatability and (d) stability measurements of the 1NTO sensors to 500 ppm ethanol at 320 °C.

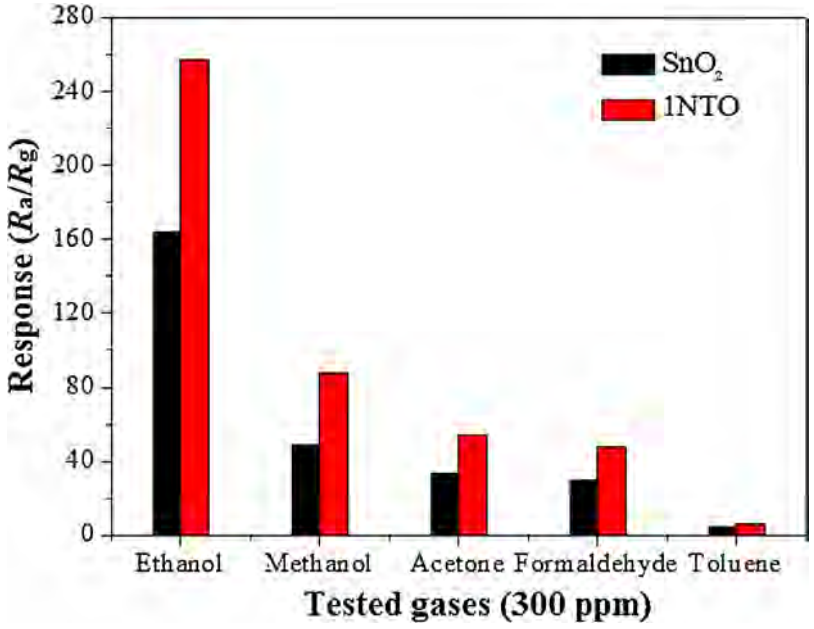

Fig. 12. Responses of SnO_2 and 1NTO sensors to 300 ppm different reducing gases at 320 °C.

p-NiO/n-SnO_2 junctions were successfully created in the composite materials. The concentration gradient of charge carriers at the heterojunction interface will impel electrons to transfer from SnO_2 to NiO and holes from NiO to SnO_2 until the system obtains equalization at the Fermi level (Fig. 13c). As a result, besides of the EDL formed by absorbed oxygen, an additional EDL can be also formed on the surface of SnO_2, as shown in Fig. 13b. Because the NiO content in the NiO/SnO_2 composites is very low, the sensor resistance

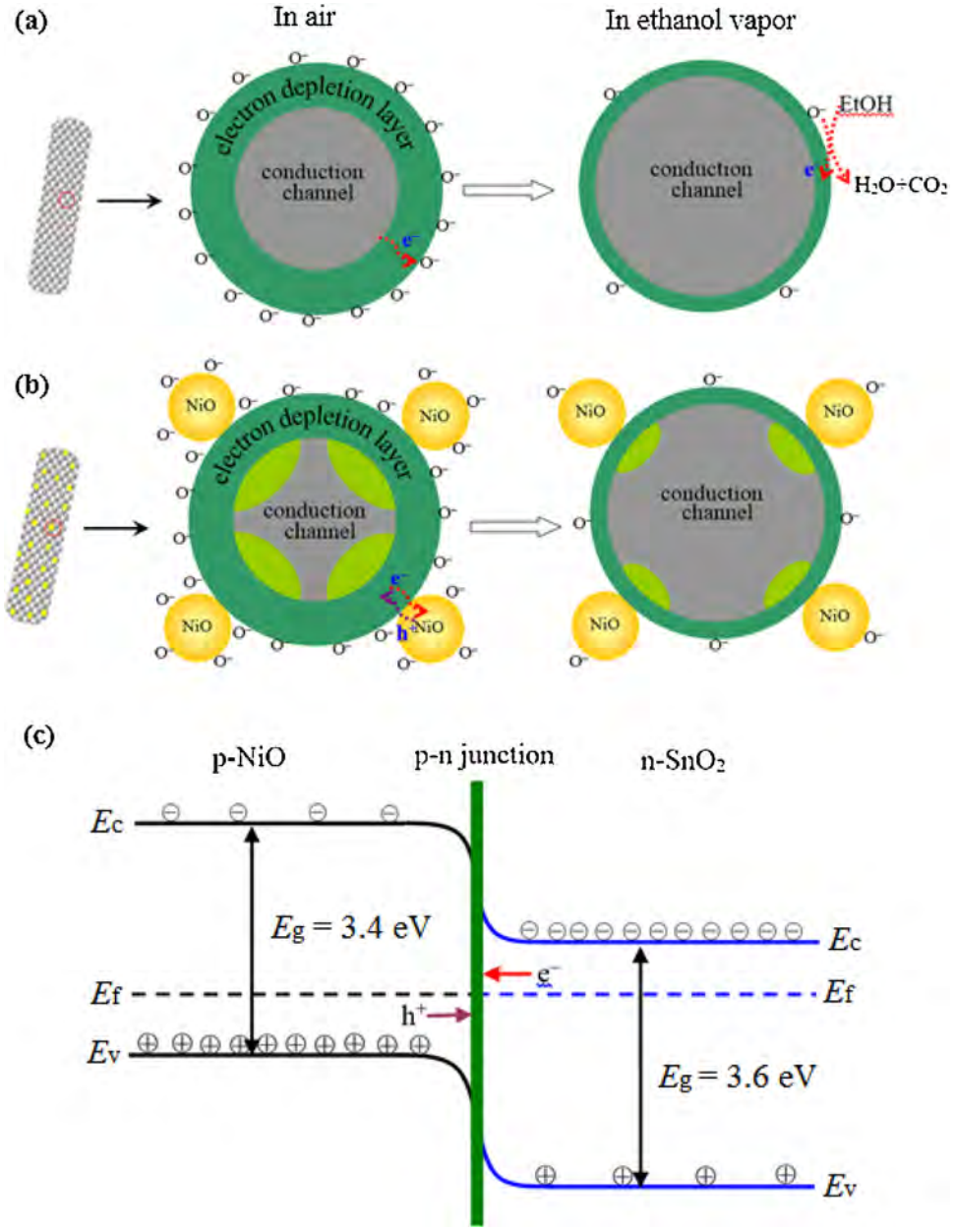

Fig. 13. Schematic diagrams of the ethanol sensing mechanisms of (a) pure SnO_2 and (b) heterostructured NiO/SnO_2 porous nanorods, and (c) the proposed energy band structure diagram of p-NiO/n-SnO_2 heterojunction.

should be mainly determined by the dominant SnO_2 phase. Thus, with the increase of EDL width on SnO_2 NPs, a higher resistance is obtained. Such deduction can be proved by the experimental result showed in Fig. 9b. The measured electrical resistance of 1NTO in air at 320 °C is about 214 KΩ, which is about two times larger than that of pure SnO_2 (about 100 KΩ). When the NiO/SnO_2 sensors are exposed to ethanol vapor, the captured electron by oxygen anions and NiO will feed back to SnO_2 due to the surface redox reaction, which will decrease the barrier height of p-n junction, shrink the EDL and widen the conduction channel of SnO_2 (Fig. 13b). As a result, the conductivity of NiO/SnO_2 sensor is significantly increased and the sensitivity is remarkably improved. Besides of the p-NiO/n-SnO_2 junctions, the porous structure is also considered to have a positive influence on the enhanced response of NiO/SnO_2 by providing a great number of channels for gas diffusion and transport as well as more active sites for gas adsorption and surface reaction, which has be widely demonstrated in previous literature [23,24].

4. Conclusion

In summary, NiO-decorated SnO_2 microflowers, consisting of porous nanorods as building blocks, have been successfully prepared by annealing pre-synthesized SnC_2O_4 sacrificial template with $Ni(NO_3)_2$. Through this method, NiO NPs can be homogenously dispersed in porous SnO_2 NRs and the NiO content can be precisely controlled by adjusting the amount of $Ni(NO_3)_2$. The optimal NiO content in the present NiO/SnO_2 composite is determined to be 1 mol%. The sensor based on 1NTO exhibit remarkably enhanced response to ethanol as compared with that based on the pure SnO_2, which can be attribute to the formation of NiO-SnO_2 p-n heterojunctions. Our research not only provides a reliable route for synthesizing porous nanorods-assembled NiO/SnO_2 heterostuctured microflowers but also demonstrates that constructing porous structure and p-n heterojunctions in SnO_2 is a feasible and effective method for achieving high gas sensing performance.

Acknowledgements

This work was supported by the National Natural Science Foundation of China (U1304520, 51172065), Program for Innovative Research Team in the University of He'nan Province (2012IRTSTHN007), Foundation of He'nan Scientific and Technology key project (13210221051), and the Education Department Natural Science Foundation of fund He'nan province (13A430135).

References

[1] J. Lee, Gas sensors using hierarchical and hollow oxide nanostructures: overview, Sens. Actuators B 140 (2009) 319–336.
[2] H. Kim, J. Lee, Highly sensitive and selective gas sensors using p-type oxide semiconductors: overview, Sens. Actuators B 192 (2014) 607–627.
[3] Y. Zhang, J. Yin, L. Li, L. Zhang, L. Bie, Enhanced ethanol gas-sensing properties of flower-like p-CuO/n-ZnO heterojunction nanorods, Sens. Actuators B 202 (2014) 500–507.
[4] F. Yang, Z. Guo, Comparison of the enhanced gas sensing properties of tin dioxide samples doped with different catalytic transition elements, J. Colloid Interface Sci. 448 (2015) 265–274.
[5] W.D. Lou, L.A. Archer, Z. Yang, Hollow micro-/nanostructures: synthesis and applications, Adv. Mater. 20 (2008) 3987–4019.
[6] P. Manjula, R. Boppella, S.V. Manorama, A facile and green approach for the controlled synthesis of porous SnO_2 nanospheres: application as an efficient photocatalyst and an excellent gas sensing material, ACS Appl. Mater. Interfaces 4 (2012) 6252–6260.
[7] Y.J. Hong, M.Y. Son, Y.C. Kang, One-pot facile synthesis of double-Shelled SnO_2 yolk-shell-structured powders by continuous process as anode materials for Li-ion batteries, Adv. Mater. 25 (2013) 2279–2283.
[8] Z. Wang, D. Luan, F.Y.C. Boey, X.W.D. Lou, Fast formation of SnO_2 nanoboxes with enhanced lithium storage capability, J. Am. Chem. Soc. 133 (2011) 4738–4741.
[9] C. Guan, X. Wang, Q. Zhang, Z. Fan, H. Zhang, H.J. Fan, Highly stable and reversible lithium storage in SnO_2 nanowires surface coated with a uniform hollow shell by atomic layer deposition, Nano Lett. 14 (2014) 4852–4858.
[10] X.C. Dou, D. Sabba, N. Mathews, L.H. Wong, Y.M. Lam, S. Mhaisalkar, Hydrothermal synthesis of high electron mobility Zn-doped SnO_2 nanoflowers as photoanode material for efficient dye-sensitized solar cells, Chem. Mater. 23 (2011) 3938–3945.
[11] J. Xing, W.Q. Fang, Z. Li, H.G. Yang, TiO_2-coated ultrathin SnO_2 nanosheets used as photoanodes for dye-sensitized solar cells with high efficiency, Ind. Eng. Chem. Res. 51 (2012) 4247–4253.
[12] H. Wang, A.L. Rogach, Hierarchical SnO_2 nanostructures: recent advances in design, synthesis, and applications, Chem. Mater. 26 (2014) 123–133.
[13] C.J. Martinez, B. Hockey, C.B. Montgomery, S. Semancik, Porous tin oxide nanostructured microspheres for sensor applications, Langmuir 21 (2005) 7937–7944.
[14] J.T. McCue, J.Y. Ying, SnO_2-In_2O_3 nanocomposites as semiconductor gas sensors for CO and NO_x detection, Chem. Mater. 19 (2007) 1009–1015.
[15] M. Epifani, J. Arbiol, E. Pellicer, E. Comini, P. Siciliano, G. Faglia, J.R. Morante, Synthesis and gas-sensing properties of Pd-doped SnO_2 nanocrystals. a case study of a general methodology for doping metal oxide nanocrystals, Cryst. Growth Des. 8 (2008) 1774–1778.
[16] F. Gyger, M. Hübner, C. Feldmann, N. Barsan, U. Weimar, Nanoscale SnO_2 hollow spheres and their application as a gas-sensing material, Chem. Mater. 22 (2010) 4821–4827.
[17] H. Zhang, W. Zeng, J. Hao, Y. Li, B. Miao, Hydrothermal synthesis of flower-like SnO_2 architectures with superior gas sensing properties, Mater. Lett. 145 (2015) 133–136.
[18] L. Wang, S. Wang, Y. Wang, H. Zhang, Y. Kang, W. Huang, Synthesis of hierarchical SnO_2 nanostructures assembled with nanosheets and their improved gas sensing properties, Sens. Actuators B 188 (2013) 85–93.
[19] M.D. Arienzo, D. Cristofori, R. Scotti, F. Morazzoni, New insights into the SnO_2 sensing mechanism based on the properties of shape controlled tin oxide nanoparticles, Chem. Mater. 25 (2013) 3675–3686.
[20] S. Wang, J. Yang, H. Zhang, Y. Wang, X. Gao, L. Wang, Z. Zhu, One-pot synthesis of 3D hierarchical SnO_2 nanostructures and their application for gas sensor, Sens. Actuators B 207 (2015) 83–89.
[21] A. Gurlo, Nanosensors: towards morphological control of gas sensing activity. SnO_2, In_2O_3, ZnO and WO_3 case studies, Nanoscale 3 (2011) 154–165.
[22] H. Wang, J. Liang, H. Fan, B. Xi, M. Zhang, S. Xiong, Y. Zhu, Y. Qian, Synthesis and gas sensitivities of SnO_2 nanorods and hollow microspheres, J. Solid State Chem. 181 (2008) 122–129.
[23] J. Huang, L. Wang, C. Gu, Z. Wang, Y. Sun, J. Shim, Preparation of porous SnO_2 microcubes and their enhanced gas-sensing property, Sens. Actuators B 207 (2015) 782–790.
[24] P. Jin, X. Zou, L. Zhou, J. Zhao, H. Chen, Y. Tian, G. Li, Biopolymer-assisted construction of porous SnO_2 microspheres with enhanced sensing properties, Sens. Actuators B 204 (2014) 142–148.
[25] J. Huang, K. Yu, C. Gu, M. Zhai, Y. Wu, M. Yang, J. Liu, Preparation of porous flower-shaped SnO_2 nanostructures and their gas-sensing property, Sens. Actuators B 147 (2010) 467–474.
[26] S. Liu, Y. Zhang, B. Yu, Z. Wang, H. Zhao, N. Zhou, T. Zhang, Solvent-free infiltration method to prepare mesoporous SnO_2 templated by SiO_2 nanoparticles for ethanol sensing, Sens. Actuators B 210 (2015) 700–705.
[27] K. Xu, D. Zeng, S. Tian, S. Zhang, C. Xie, Hierarchical porous SnO_2 micro-rods topologically transferred from tin oxalate for fast response sensors to trace formaldehyde, Sens. Actuators B 190 (2014) 585–592.
[28] Y. Zong, Y. Cao, D. Jia, P. Hu, The enhanced gas sensing behavior of porous nanocrystalline SnO_2 prepared by solid-state chemical reaction, Sens. Actuators B 145 (2010) 84–88.
[29] S. Choi, A. Katoch, J. Kim, S.S. Kim, Prominent reducing gas-sensing performances of n-SnO_2 nanowires by local creation of p-n heterojunctions by functionalization with p-Cr_2O_3 nanoparticles, ACS Appl. Mater. Interfaces 6 (2014) 17723–17729.
[30] D. Ju, H. Xu, Q. Xu, H. Gong, Z. Qiu, J. Guo, J. Zhang, B. Cao, High triethylamine-sensing properties of NiO/SnO_2 hollow sphere P-N heterojunction sensors, Sens. Actuators B 215 (2015) 39–44.
[31] N. Van Hieu, P. Thi Hong Van, L. Tien Nhan, N. Van Duy, N. Duc Hoa, Giant enhancement of H_2S gas response by decorating n-type SnO_2 nanowires with p-type NiO nanoparticles, Appl. Phys. Lett. 101 (2012) 253106.
[32] G. Sun, F.X. Qi, S.S. Zhang, Y.W. Li, Y. Wang, J.L. Cao, H. Bala, X.D. Wang, T.K. Jia, Z.Y. Zhang, Synthesis and enhanced gas sensing properties of flower-like SnO_2 hierarchical structures decorated with discrete ZnO nanoparticles, J. Alloys Compd. 617 (2014) 192–199.
[33] X.C. Ma, H.Y. Song, C.S. Guan, Enhanced ethanol sensing properties of ZnO-doped porous SnO_2hollow nanospheres, Sens. Actuators B: Chem. 188 (2013) 193–199.
[34] Q. Yu, J. Zhu, Z. Xu, X. Huang, Facile synthesis of α-Fe_2O_3@SnO_2 core–shell heterostructure nanotubes for high performance gas sensors, Sens. Actuators B 213 (2015) 27–34.
[35] F. Shao, M.W.G. Hoffmann, J.D. Prades, R. Zamani, J. Arbiol, J.R. Morante, E. Varechkina, M. Rumyantseva, A. Gaskov, I. Giebelhaus, T. Fischer, S. Mathur, F. Hernández-Ramírez, Heterostructured p-CuO (nanoparticle)/n-SnO_2 (nanowire) devices for selective H_2S detection, Sens. Actuators B 181 (2013) 130–135.
[36] Y.J. Wang, Q.S. Wang, X.Y. Zhan, F.M. Wang, M. Safdar, J. He, Visible light driven type II heterostructures and their enhanced photocatalysis properties: a review, Nanoscale 5 (2013) 8326–8339.
[37] Y.F. Sun, S.B. Liu, F.L. Meng, J.Y. Liu, Z. Jin, L.T. Kong, J.H. Liu, Metal oxide nanostructures and their gas sensing properties: a review, Sensors 12 (2012) 2610–2631.
[38] L. Liu, Y. Zhang, G.G. Wang, S.C. Li, L.Y. Wang, Y. Han, X.X. Jiang, A.G. Wei, High toluene sensing properties of NiO–SnO_2 composite nanofiber sensors operating at 330 °C, Sens. Actuators B 160 (2011) 448–454.
[39] H. Liu, J. Zhang, X.Z. Guo, S.H. Wu, S.R. Wang, Enhanced sensor response of Ni-doped SnO_2 hollow spheres, Sens. Actuators B 152 (2011) 162–167.
[40] Y.G. Zheng, J. Wang, P.J. Yao, Formaldehyde sensing properties of electrospun NiO-doped SnO_2 nanofibers, Sens. Actuators B: Chem. 156 (2011) 723–730.
[41] L.L. Wang, J.N. Deng, T. Fei, T. Zhang, Template-free synthesized hollow NiO–SnO_2 nanospheres with high gas-sensing performance, Sens. Actuators B 164 (2012) 90–95.

Biographies

Guang Sun received his PhD degree in materials science in 2007 from Yanshan University, China. He is currently an associate professor in the School of Materials Science and Engineering of Henan Polytechnic University, China. His research interests include the design and synthesis of nanostructured metal oxide semiconducting materials and their applications in catalyst, gas sensor and lithium ion rechargeable battery.

Honglin Chen received her BS degree in 2014. She is currently a master course student at Henan Polytechnic University. Her major is materials physics and chemistry.

Yanwei Li received her master's degree in 2002 from Hebei University, China. She is currently a lecture in Henan Polytechnic University, China. Her research focus is on the design and synthesis of metal oxide nanostructures and their application in gas sensor.

Zehua Chen received his PhD degree in Chemistry in 2014 from Central South University, China. Presently he is a researcher in the School of Materials Science and Engineering of Henan Polytechnic University, China. In 2011 he went to Professor M. Stanley Whittingham's research group in the Materials Science Department at State University of New York at Binghamton as a joint-PhD to study chemistry material. His research interests focus on the design and synthesis of nanostructured metal oxide semiconducting materials and their applications in catalyst, gas sensor and lithium ion rechargeable battery.

Saisai Zhang received her BS degree in 2013. She is currently a master course student at Henan Polytechnic University. Her major is materials physics and chemistry.

Guangzhou Ma received his BS degree in 2015. He is currently a master course student at Henan Polytechnic University. His major is materials physics and chemistry.

Tiekun Jia received his PhD degree of Chemistry in 2009 from Wuhan University of Technology, China. He is currently an associate professor in the Department of Materials Science and Engineering of Luoyang Institute of Science and Technology, China. His research topic is the synthesis of nanostructured metal oxide materials and their applications in catalyst and gas sensor.

Jianliang Cao received his PhD degree of Chemistry in 2009 from Nankai University, China. He is currently an associate professor in the School of Materials Science and Engineering of Henan Polytechnic University, China. His research topic is the synthesis of nanostructured metal oxide materials and their applications in catalyst and gas sensor.

Hari Bala received his PhD degree of materials science in 2005 from Jilin University, China. Now, he is a professor in the School of Materials Science and Engineering of Henan Polytechnic University, China. His research interests are focused on controlled synthesis of nanostructured metal oxide materials and their applications in gas sensor and dye-sensitized solar cell.

Zhanying Zhang received his PhD degree of materials science and engineering in 1982. Now, he is a professor and the vice-president of Henan Polytechnic University, China. His research interests are focused on the design, synthesis and application of nanostructured metal oxide semiconducting materials.